Atmospheric
Measurement
Techniques
Discussions

1 Theoretical Derivation of Aerosol Lidar Ratio using Mie
2 Theory for CALIOP-CALIPSO and OPAC Aerosol Models

3 Radhika A. Chipade[1] and Mehul R. Pandya[1]

4 [1]Space Applications Centre (ISRO), Ahmedabad, Gujarat, India – 380015.

5 *Correspondence to*: Radhika A. Chipade (radhikachipade@gmail.com)

6 **Abstract.** The extinction-to-backscattering ratio, popularly known as lidar (light detection and ranging) ratio of

7 atmospheric aerosols is an important optical property, which is essential to retrieve the extinction profiles of

8 atmospheric aerosols. Lidar satellite observations can provide the global coverage of atmospheric aerosols along

9 with their vertical extent. NASA's Cloud-Aerosol Lidar with Orthogonal Polarisation (CALIOP) on-board Cloud-

10 Aerosol Lidar and Infrared Pathfinder Satellite Observations (CALIPSO) is the only space-based platform

11 available so far, that provides the vertical profiles of extinction due to atmospheric aerosols. A physics-based

12 theoretical approach is presented in the present paper that estimates lidar ratio values for CALIPSO aerosol

13 models, which can be used as inputs to determine the extinction profiles of aerosols using CALIPSO data. The

14 developed methodology was also qualified by comparing it with the lidar ratio values derived using AERONET

15 datasets. Lidar ratio for CALIPSO aerosols models were estimated in the range of 38.72 sr to 85.98 sr at 532 nm

16 whereas, at 1064 nm lidar ratio varied between 20.11 sr to 71.11 sr depending upon the aerosol type and their size

17 distributions.

18 Aerosols are compositions of various particles and thus the presence of water vapour in the atmosphere can affect

19 the optical properties of the aerosols. Thus, the effect of relative humidity on lidar ratio was studied using Optical

20 Properties of Cloud and Aerosols software tool (OPAC) aerosol models, which are the standard aerosol models

21 against the cluster classified AERONET and CALIPSO aerosol models. Water soluble particles contribute

22 substantially in clean continental, clean marine, tropical marine and desert aerosol models and are hygroscopic in

23 nature. Hygroscopic sulfate particles dominate the Antarctic aerosols during summertime. In presence of relative

24 humidity between 0 – 80%, the lidar ratio values were observed to decrease from 53.59 sr to 47.13 sr, 53.66 sr to

25 47.15 sr, 53.70 sr to 47.16 sr and 55.32 sr to 48.78 sr at 532 nm for clean continental, clean marine, tropical marine

26 and desert aerosols respectively, whereas lidar ratio gradually increased from 47.13 sr to 51 sr, 47.15 sr to 51 sr,

27 47.16 sr to 51 sr and 48.78 sr to 51.68 sr respectively for these aerosol models when relative humidity was between

28 80 – 99%; due to constituent hygroscopic particles. In case of Antarctic aerosols, the lidar ratio was observed to

29 increase from 57.73 sr to 97.64 sr due to hygroscopic sulfate particles that backscattered heavily in presence of

30 water vapour at 532 nm. The soot particles dominate the polluted continental and polluted marine particles causing

31 an increase in lidar ratio over corresponding clean counterpart. Similar results were observed at 1064 nm for

32 OPAC aerosol models.

33 1 Introduction:

34 The light detection and ranging (lidar) measurements are considered appropriate to retrieve the range-resolved

35 values of vertical backscatter and extinction profiles of tropospheric aerosols. The single scattering lidar equation

36 is solved in order to determine extinction and backscatter profiles of aerosols, which depends on the ratio of

Atmospheric
Measurement
Techniques
Discussions

37   extinction-to-backscatter coefficient, known as lidar ratio. Thus, estimation of lidar ratio is essential to solve the

38   lidar equation and important in the study of climatic impact of aerosols.

39   Many researchers have reported the lidar ratio estimation as a part of retrieval of extinction and backscatter profiles

40   of tropospheric aerosols using ground as well as satellite data. Takamura et al. (1994) derived lidar ratio combining

41   the measurements from lidar, sunphotometer and optical particle counter. Lidar ratio can be directly estimated

42   using the Raman lidar. Ansmann et al. (2002) demonstrated that the lidar ratio retrieved using Raman lidar can be

43   used to retrieve extinction profiles of the aerosols using elastic backscatter lidar. The National Aeronautics And

44   Space Administration's (NASA's) Cloud-Aerosol Lidar with Orthogonal Polarisation (CALIOP) on-board Cloud-

45   Aerosol Lidar and Infrared Pathfinder Satellite Observations (CALIPSO) launched in 2006 is the only available

46   source of satellite data to retrieve vertical profiles of tropospheric aerosols. CALIOP is an elastic backscatter lidar

47   (Hunt et al. 2009) that records the backscatter photon counts due to tropospheric aerosols and the vertical

48   extinction and backscatter profiles of aerosols are retrieved solving the single scattering lidar equation (Young

49   and Vaughan 2009). This retrieval process uses a look-up table approach for lidar ratio in order to solve the lidar

50   equation. The lidar ratio selection scheme used for CALIOP-CALIPSO products is based on cluster analysis of

51   aerosol measurements using data recorded at several AERONET network stations spread across the globe (Omar

52   et al. 2009, Young and Vaughan 2009). Thus, a novel theoretical approach is presented in the present paper to

53   retrieve the lidar ratio for CALIOP-CALIPSO aerosol models.

54   The lidar ratio depends on two optical properties viz. extinction coefficient and backscattering coefficinet and

55   thus, it depends on the incident wavelength, refractive index and the size distribution of the aerosols. In real

56   atmospheric conditions, aerosols exhibit different shapes and sizes and are composed of various kinds of

57   compounds. In addition to this, various aerosol components are affected due to variations in relative humidity.

58   Thus, it is essential to study the variations in lidar ratio due to different atmospheric conditions for various

59   compositions of aerosols. Salemink et al. (1984) reported a linear increase in the lidar ratio when relative humidity

60   was increased from 40% to 80% during a field experiment details of which are not mentioned in the paper.

61   Ackermann (1998) has reported a numerical study of lidar ratio with respect to variations in relative humidity for

62   Nd:YAG wavelengths for continental, maritime and desert aerosol models where author has considered some

63   hypothetical cases for number mixing ratios of the aerosol components. He has established a non-linear

64   relationaship between relative humidity and lidar ratio. Zhao et al. (2017) used Mie theory and k-Kohler theory

65   to study the influences of aerosol hygroscopic growth on lidar ratio and used *in-situ* data collected during a field

66   campaign to establish a relationship between lidar ratio and relative humidity. Dusing et al. (2021) has also

67   established a non-linear relationship between lidar ratio and relative humidity for Central European aerosols using

68   *in-situ* data. Optical properties of aerosols are important to study the radiation balance of the Earth and climate

69   change. Optical Properties of Cloud and Aerosols (OPAC) software tool facilitates with the dataset of optical

70   properties of the aerosols and clouds and a program to extract these datasets. The standard global aerosol models

71   are considered in OPAC as given in d'Almeida et al. (1991) and Hess et al. (1998). Component mixing in aerosols

72   is based on particle number densities, which are independent of relative humidities in OPAC. However, this will

73   affect the aerosol lidar ratio.

74   Several authors have reported different lidar ratio values for different aerosol models using a variety of

75   methodologies. d'Almeida et al. (1991) have reported values of 16-22 sr for clean marine and desert models at

76   ruby wavelength when lidar ratio was estimated as ratio of extinction coefficient to phase function at 180°. They

Atmospheric
Measurement
Techniques
Discussions

77   have reported a value up to 80 sr for Antarctic aerosols at ruby wavelength. Anderson et al. (2000) have showed

78   a variation of 8 to 95 sr in lidar ratio values for polluted continental model at 532 nm using nephelometer data.

79   Omar et al. (2009) have reported lidar ratio values for desert, smoke, clean continental, polluted continental, clean

80   marine and polluted dust aerosols at 532 nm and 1064 nm varying between 20-70 sr using AERONET data. These

81   values are reported with 30% uncertainty and are selected as lidar ratio in CALIPSO-V1 operational algorithms.

82   The lidar ratios for polluted dust aerosols are updated to 55 sr and 48 sr at 532 nm and 1064 nm respectively, in

83   CALIPSO-V3 operational algorithm whereas lidar ratio for clean continental aerosols is updated to 53 sr at 532

84   nm in CALIPSO-V4 operational algorithm (Kim et al. 2018). Lopes et al. (2013) have reported a regional study

85   in Brazil about lidar ratio selection algorithm for CALIPSO data only at 532 nm using AERONET sun

86   photometers. They have reported the similar values for all aerosol models as used in CALIPSO-V1 algorithm by

87   Omar et al. (2009) except for polluted dust in which case the lidar ratio value is updated to 55 sr. Li et al. (2022)

88   have assessed CALIPSO-V4 lidar ratio selection algorithm by retrieving lidar ratios as combination of CALIPSO

89   columnar attenuated backscatter and Synergised Optical Depth of Aerosols (SODA) algorithms. This study has

90   ignored clean continental aerosols and has proposed elevated smoke and dusty marine aerosol models with lidar

91   ratios of 47 sr and 32 sr respectively; during night at 532 nm.

92   The present study reports a theoretical approach for estimation of lidar ratio from various sources, such as aerosol

93   models reported by Hess et al. (1998) (OPAC aerosol models), Omar et al. (2005 and 2009) for wavelengths 532

94   nm, 673 nm and 1064 nm (CALIPSO and AERONET aerosol models). The variation in lidar ratio with respect to

95   relative humidity was also studied at Nd:YAG wavelengths using OPAC (Hess et al. 1998) aerosol models. Hess

96   et al. (1998) have reported aerosol models as composition of various components contributing to different aerosol

97   types whereas Omar et al. (2005 and 2009) have reported aerosol models in terms of contribution from fine and

98   coarse particles i.e. in terms of aerosol sizes. As mentioned earlier, theoretical approach for lidar ratio estimation

99   using Mie theory is still a gap area for CALIPSO and OPAC aerosol models and thus, this study, attempts to

100   provide a physics based theoretical approach covering all types of aerosol models over the varying lidar ratio

101   values based on in-situ measurements.

102   The paper is organised into five sections. The first section presents the introductory literature review and

103   motivation behind this study. The second section outlines the data used in this study. The detailed methodology

104   and Mie theory for lidar ratio estimation is presented in the third section of this paper. The results are discussed

105   in the fourth section whereas the concluding remarks are listed in the fifth section of this paper.

106   **2   Input Data:**

107   The lidar ratio depends on aerosol size distribution, refractive index and incident wavelength. The inputs used in

108   this study are the aerosol models provided in d'Almeida et al. (1991), Ackermann (1998), Hess et al. (1998), and

109   Omar et al. (2005 and 2009).

110   Table 1 and 2 present the CALIOP-CALIPSO aerosol models and cluster classified AERONET aerosol models

111   respectively; defined in Omar et al. (2009 and 2005) at 532 nm, 673 nm and 1064nm. These data include the

112   refractive indices (in terms of real part (m_r) and imaginary part (m_i)) for each of the component aerosols along

113   with the size distribution of the aerosol in terms of median radius (r_m) and standard deviation (σ).

Atmospheric
Measurement
Techniques
Discussions

114   Omar et al. (2005) have reported aerosol refractive indices at 673 nm and have classified aerosols through cluster

115   analysis in six different categories numbered 1-6 viz. desert dust, biomass burning, rural, industrial pollution,

116   polluted marine and dirty pollution using AERONET data. The desert dust and polluted marine (i.e. category 1

117   and category 5) aerosol models represent the categories of aerosols originated from the natural sources whereas

118   the biomass burning, continental pollution and dirty pollution (i.e. category 2, 4, and 6) aerosol models represent

119   the aerosols emanating from the anthropogenic sources. Rural background aerosol model (i.e. category 3)

120   represent those aerosols which are observed in relatively clean atmosphere.

121   The category 1 aerosols have fine fraction by volume of 0.22 indicating that coarse particles dominate the volume

122   of this category. The mean radius and geometric standard deviation for the fine mode is of 0.12 µm and 1.48 µm

123   respectively; for this category. The refractive index of this category of aerosols is considered to be $1.45 - 0.0036i$

124   as reported in table 2. The sites considered for these category of aerosols are either desert regions, close to desert

125   regions or the sites where desert dust has been observed as a result of long-range transport. The category 2 aerosols

126   have fine fraction by volume of 0.33 whereas mean and geometric standard deviation for the fine mode is 0.14

127   µm and 1.56 µm respectively. Category 2 aerosols are dominated by coarse mode particles which have a mean

128   radius and geometric standard deviation of 3.73 µm and 2.14 µm respectively. Category 1 and category 2 aerosols

129   have single scattering albedo values of 0.94 and 0.82 respectively which are estimated using Mie theory presented

130   in this paper. These single scattering albedo values are consistent with those reported by Omar et al. (2005).

131   Category 3 aerosols are characterised by low optical depth values as they are originated from clean atmosphere.

132   These aerosols have fine fraction by volume of 0.38 indicating dominance of coarse particles. The mean radius

133   and geometric standard deviation for the fine mode is of 0.13 µm and 1.50 µm respectively. The refractive index

134   for this category of aerosols is considered to be $1.45 - 0.0092i$. The single scattering albedo value is observed to

135   0.89 for category 3 aerosols. The category 4 aerosols are found in urban centres or near urban centres and are

136   dominated by the natural pollutants such as sulfate particles (Omar et al. 2005). The refractive index for these

137   category of aerosols is considered to be $1.41 - 0.0063i$ which is representing the natural pollutants comprising

138   category 4 aerosols. The size distribution of category 4 aerosols is described by a mean radius and geometric

139   standard deviation for fine mode of 0.16 µm and 1.53 µm respectively. The mean radius and geometric standard

140   deviation for coarse mode is of 3.55 µm and 2.07 µm respectively. The single scattering albedo for these category

141   of aerosols is estimated to be 0.93.

142   The category 5 aerosols are observed at islands or at coastal regions. The fine fraction by volume is of 0.26 and

143   size distribution is described by a mean radius and geometric standard deviation for fine mode of 0.17 µm and

144   1.61 µm respectively. The refractive index for these category of aerosols is considered to be $1.39 - 0.0044i$. These

145   optical properties are resulted in the single scattering albedo of 0.94 for polluted marine aerosols. The category 6

146   aerosols are similar to category 4 aerosols with a high imaginary part of refractive index. The refractive index of

147   category 6 aerosols is considered to be $1.41 - 0.0337i$ which resulted in low single scattering albedo of 0.68. The

148   low single scattering albedo indicates that these are the aerosols with mostly carbon element in it (Omar et al.

149   2005). The size distribution of these category of aerosols is described by a mean radius and geometric standard

150   deviation of 0.14 µm and 1.54 µm respectively. The more details about these six categories of aerosols can be

151   found in Omar et al. (2005).

Atmospheric
Measurement
Techniques
Discussions

152 The theoretically derived lidar ratios were compared with lidar ratio derived using AERONET data for three

153 different stations classified for each of the above-mentioned six categories. The details are discussed in results

154 section of this paper.

155 Table 3, 4 and 5 collectively report the OPAC aerosol models. These aerosol models are defined in terms of their

156 size distribution with respect to relative humidity, refractive indices at 532 nm and 1064 nm and composition of

157 aerosol types in terms of number mixing ratio (μ). The lognormally distributed aerosol components were

158 considered in this study. The relative humidity was varied from 0% to 99% with intermediate steps at 50%, 70%,

159 80%, 90% and 98%. The details about OPAC aerosol models can be found in Hess et al. (1998).

160 ## 3   Computation of Lidar Ratio using Mie Theory:

161 In this study, the aerosols were assumed as homogeneous isotropic spheres scattering the electromagnetic

162 radiation incident upon them. These scattering phenomenons are modelled using Mie theory, which is discussed

163 in Bohren, and Huffman (1983) and Vermote et al. (2006) and many other authors. The lidar ratio, which is defined

164 as the ratio of extinction coefficient to backscatter coefficient, is derived in the present study using the Mie theory

165 equations. The computational equations are presented here briefly, for the ready reference.

166 The Mie parameter (x) for an aerosol with refractive index, $m = n_r - in_i$; is defined as

167 $$x = \frac{2\pi r}{\lambda},$$ (1)

168 where r is the aerosol particle radius in micron and λ is the wavelength in micron. Here m is the refractive index

169 with real part n_r and imaginary part n_i.

170 Two complex functions $S_1(x, m, \theta)$ and $S_2(x, m, \theta)$ related to amplitude of scattered radiation that are

171 perpendicular and parallel to the plane of scattering with scattering angle θ, respectively, can be defined as

172 follows.

173 $$S_1(x, m, \theta) = \sum_{n=1}^{\infty} \frac{(2n+1)}{n(n+1)} [a_n(x, m)\pi_n(cos\theta) + b_n(x, m)\tau_n(cos\theta)] \text{ and}$$ (2)

174 $$S_2(x, m, \theta) = \sum_{n=1}^{\infty} \frac{(2n+1)}{n(n+1)} [a_n(x, m)\tau_n(cos\theta) + b_n(x, m)\pi_n(cos\theta)],$$ (3)

175 where, the complex functions $a_n(x, m)$ and $b_n(x, m)$ are given by

176 $$a_n(x, m) = \frac{\Psi'_n(mx)\Psi_n(x) - m\Psi_n(mx)\Psi'_n(x)}{\Psi'_n(mx)\xi_n(x) - m\Psi_n(mx)\xi'_n(x)} \text{ and}$$ (4)

177 $$b_n(x, m) = \frac{m\Psi'_n(mx)\Psi_n(x) - \Psi_n(mx)\Psi'_n(x)}{m\Psi'_n(mx)\xi_n(x) - \Psi_n(mx)\xi'_n(x)},$$ (5)

178 which are defined in terms of Ricatti-Bessel functions $\Psi_n(z = x \text{ or } mx)$ and $\xi_n(z = x \text{ or } mx)$. Ricatti-Bessel

179 functions are evaluated using their logarithmic derivatives details of which are provided in Vermote et al. (2006).

180 In order to compute the complex functions $S_1(x, m, \theta)$ and $S_2(x, m, \theta)$, the functions π_n and τ_n are computed

181 using associated Legendre polynomials. The functions π_n and τ_n are the functions of scattering angle θ. These

182 can be computed using the recurrence relations

183 $$n\pi_{n+1}(cos\theta) = (2n + 1)cos\theta\pi_n(cos\theta) - (n + 1)\pi_{n-1}(cos\theta) \text{ and}$$ (6)

184 $$\tau_{n+1}(cos\theta) = (n + 1)cos\theta\pi_{n+1}(cos\theta) - (n + 2)\pi_n(cos\theta).$$ (7)

185 which are initialised with $\pi_0(cos\theta) = 0$, $\pi_1(cos\theta) = 1$, and $\tau_0(cos\theta) = cos\theta$.

186 Using these quantities, the extinction efficiency $(Q_e(\lambda, r, m))$, dimensionless angular-scattering intensity

187 efficiency $(M_{11}(\lambda, r, m, \theta))$, the scattering efficiency $(Q_{sca}(\lambda, r, m))$, and backscattering efficiency

188 $(Q_{back}(\lambda, r, m))$ can be computed as

189 $Q_e(\lambda, r, m) = \frac{\sigma_e(\lambda, r, m)}{\pi r^2} = \frac{2}{x^2}\sum_{n=1}^{\infty}(2n+1)\mathcal{R}e[a_n(x, m) + b_n(x, m)],$ (8)

190 $M_{11}(\lambda, r, m, \theta) = \frac{1}{2x^2}[S_1(x, m, \theta)S_1^*(x, m, \theta) + S_1(x, m, \theta)S_2^*(x, m, \theta)],$ (9)

191 $Q_{sca}(\lambda, r, m) = \frac{\sigma_{sca}(\lambda, r, m)}{\pi r^2} = \frac{2}{x^2}\sum_{n=1}^{\infty}(2n+1)[a_n(x, m)a_n^*(x, m) + b_n(x, m)b_n^*(x, m)]$ and (10)

192 $Q_{back}(\lambda, r, m) = \frac{4}{x^2}|S_1(x, m, 180^0)|^2 = 4M_{11}(\lambda, r, m, 180^0),$ (11)

193 where r is the particle radius, $\sigma_e(\lambda, r, m)$ is the extinction cross section and $\sigma_{sca}(\lambda, r, m)$ is the scattering cross

194 section.

195 Thus, the lidar ratio can be computed as

196 $LR = \frac{Nr}{Dr} = \frac{\sum_{i=1}^{M}\int_0^{\infty}Q_e(\lambda, r, m_i)\pi r^2 n(r)dr}{\sum_{i=1}^{M}\int_0^{\infty}Q_{back}(\lambda, r, m_i)\pi r^2 n(r)dr}.$ (12)

197 The single scattering albedo can be computed as

198 $\omega_0 = \frac{\sum_{i=1}^{M}\int_0^{\infty}Q_{sca}(\lambda, r, m_i)\pi r^2 n(r)dr}{\sum_{i=1}^{M}\int_0^{\infty}Q_e(\lambda, r, m_i)\pi r^2 n(r)dr}.$ (13)

199 In this study, an aerosol is considered as mixture of its constituent components. And each of the component is

200 lognormally distributed with median radius r_m and standard deviation σ. Thus,

201 $n(r) = \frac{\mu N_{tot}}{\sqrt{2\pi}r\ln(\sigma)}exp\left[-\frac{ln^2(r/r_m)}{2ln^2\sigma}\right],$ (14)

202 where μ is the number mixing ratio (i.e. normalised number particle concentration) and N_{tot} is the total number

203 density of the aerosol component.

204 The relative humidity influences the refractive index of the hygroscopic aerosol components and the effective

205 refractive index is

206 $m_i = m_w + (m_{0,i} - m_w)\left(\frac{r_{0,i}}{r_{m,i}}\right)^3,$ (15)

207 where m_w is the refractive index of the water, $m_{0,i}$ is the refractive index of the dry particle of component i and

208 $r_{0,i}$ is the median radius of the dry particle of component i.

209 The theory presented above is with the assumption of homogenous spherical isotropic aerosol particles, which

210 simplifies the computation of lidar ratio. However, if the particles are not homogenous and anisotropic then the

211 above theory may cause errors as the scattering phase function will differ to address the anisotropy. Moreover, if

212 the particles are nonhygroscopic especially when the particles are large as compared to the incident wavelength

213 then the above theory fails (Ackermann 1998).

214 **4   Results and Discussion:**

215 **4.1 Lidar Ratio for AERONET and CALIPSO Aerosol Models defined in terms of particle sizes:**

216 The aerosol models defined in terms of particle size by Omar et al. (2005 and 2009) were used to estimate the

217 lidar ratio for aerosol models used in operational algorithms of CALIOP-CALIPSO. Omar et al. (2005) used

218 cluster analysis for AERONET data to define the aerosol models at 673 nm. Table 6 shows the lidar ratio estimated

219 using the Mie theory for each of the six clusters defined by Omar et al. (2005). The maximum lidar ratio of 48.87

Atmospheric
Measurement
Techniques
Discussions

Open Access

EGU

220 sr was observed for dirty pollution type of aerosols whereas the minimum of 28.76 sr was observed for desert dust

221 kind of aerosols. The lidar ratios at 532 nm are mostly discussed in literature (Ackermann 1998, Anderson et al.

222 2000, Omar et al. 2009, Lopes et al. 2013 and Kim et al. 2018 and 2022) and scanty literature is available for lidar

223 ratios at 673 nm. Moreover, these aerosol models are derived using AERONET data. Thus, the estimated lidar

224 ratios at 673 nm were compared with those of the AERONET data.

225 The data for three different stations for each of the category was selected and aerosol lidar ratio was computed

226 using equation (12) as a multiplier of 4π. Tables 7-12 show the statistics of the lidar ratio for different AERONET

227 stations belonging to different categories. The daily averages of the lidar ratios were obtained using the

228 AERONET single scattering albedo and phase function values and were compared with the Mie theory estimated

229 values. The Mie theory estimated values were observed to comply with the observed values of lidar ratios using

230 AERONET data as the theoretically estimated values were lying in between the minimum and maximum of the

231 daily lidar ratio values. The differences in the theoretical values estimated using Mie theory and those observed

232 using AERONET data were primarily due to the refractive indices of the different aerosol types present at the

233 different AERONET stations. Omar et al. (2005) had classified the different aerosol types mentioned in section 2

234 using cluster analysis and the geographical location of these AERONET stations was also considered to be an

235 important factor while classification. Thus the composition of the aerosols observed over a period of time varied

236 resulting in the variation of the refractive indices. The theoretically computed lidar ratios were based on the

237 refractive index of the centre of the cluster analysed using AERONET data before 2002 (Omar et al. 2005) whereas

238 the AERONET stations data used in this study spanned over 1998 to 2021 leading to the differences in the

239 refractive indices of the aerosol types. The shape of the aerosol particles, their size distribution and their particle

240 density present in the atmosphere may be the secondary reasons for the differences between the theoretically

241 estimated values of lidar ratio using Mie theory and the lidar ratio computed using AERONET stations data which

242 needs further investigation.

243 The aerosol models derived using the cluster analysis by Omar et al. (2005) and their respective lidar ratios were

244 used in lidar ratio selection and feature detection algorithm of CALIOP-CALIPSO (Young and Vaughan 2009).

245 These aerosol models and their respective lidar ratios used in operational algorithms of CALIOP-CALIPSO are

246 specified in Young and Vaughan (2009). These lidar ratios were subsequently updated in the V3 and V4 CALIOP-

247 CALIPSO operational algorithms (Kim et al. 2018). The basis for lidar ratio selection algorithm for CALIOP-

248 CALIPSO operational products has been the cluster analysis using the AERONET data and thus, the lidar ratios

249 were estimated using Mie theory, which gives the physical basis for the lidar ratio selection algorithm.

250 Figure 1 and 2 show the distribution of extinction and backscatter coefficients for CALIPSO aerosol models at

251 532 nm and 1064 nm; respectively. The particle sizes were varied from 0.01 μm to 5 μm and the cut-off radius

252 for fine particles was taken to be 1 μm for all CALIPSO aerosol models except clean marine aerosols in which

253 case the fine particle radius cut-off was 0.6 μm. The maxima of extinction and backscatter coefficients at 532 nm

254 and 1064 nm, for all aerosol models except clean marine aerosols was observed between 0.07 μm to 0.4 μm. In

255 case of all aerosol models, it was observed that the contribution from fine particles was more in magnitude

256 compared to that from coarser particles at 532 nm and 1064 nm except the clean marine model. In case of clean

257 marine aerosols at 1064 nm, the coarser particles were observed to contribute significantly in magnitude to the

258 extinction coefficient as compared to fine particles producing lidar ratio value of 71 sr.

259 Table 13 shows the lidar ratio values estimated for the CALIPSO aerosol models specified in Omar et al. (2009)
260 and its comparison with the lidar ratio values selected in various versions of CALIOP-CALIPSO operational
261 algorithms. It was observed that the lidar ratio values estimated using Mie theory in present study comply with
262 the lidar ratio values reported in literature for CALIPSO operational algorithms. The lidar ratio proposed for clean
263 continental model at 532 nm in CALIPSO V4 operational algorithm was 53 ± 24 sr, allowing the variation up to
264 77 sr. The Mie theory estimate for clean continental model at 532 nm was centred on 85 sr considering the
265 refractive index of the centre cluster as provided in Omar et al. (2009). The variation in refractive index will affect
266 the lidar ratio value, which was evident when compared to OPAC aerosol models where the lidar ratio of clean
267 continental aerosols was centred on 53 sr. Similar results were observed in case of clean marine aerosols at 532
268 nm and desert dust particles at 1064 nm. In case of desert dust particles at 1064 nm the variation up to 31 sr was
269 allowed in CALISPO V4 operational algorithm whereas the present study proposed lidar ratio value of 20 sr for
270 desert dust aerosols at 1064 nm. The desert dust lidar ratio at 1064 nm proposed for CALIPSO aerosol model was
271 observed to be consistent with OPAC desert aerosol model in which case lidar ratio was observed to be centred
272 on 23 sr. These results for desert aerosols at 1064 nm comply with those reported by Ackermann (1998) where
273 dry desert aerosol lidar ratio was lying just under 20 sr. The results for OPAC aerosol models are discussed in
274 detail in the subsequent section. CALISPO operational V3 algorithm allowed variation up to 68 sr in lidar ratio
275 of clean marine aerosols at 1064 nm whereas the present study estimated the value of 71 sr for clean marine
276 aerosols at 1064 nm. The theoretically estimated lidar ratio for clean marine aerosols at 532 nm was observed to
277 be consistent with that reported in the literature. The theoretically proposed value in the present study for clean
278 marine aerosols at 532 nm was 57.31 sr whereas Li et al. (2022) reported the median value of lidar ratio for clean
279 marine aerosols of 60 sr. Thus, the Mie theory estimated lidar ratio values can provide the physical basis for the
280 CALIPSO operational algorithms and can be used as look-up table to derive the vertical extinction and backscatter
281 particulate profiles using satellite data.

282 The theoretical approach proposed in this study to estimate lidar ratio for CALIPSO aerosol models was further
283 validated through estimation of single scattering albedo at 673 nm for the aerosol models classified using
284 AERONET data as described in table 2. The single scattering albedo values for AERONET aerosol models viz.
285 Category 1 to Category 6 were estimated using the above presented Mie theory as 0.94, 0.82, 0.89, 0.93, 0.94 and
286 0.68 respectively. The single scattering values at 673 nm for these AERONET aerosol models viz. Category 1 to
287 Category 6 were reported by Omar et al. (2005) as 0.93, 0.80, 0.88, 0.92, 0.93 and 0.72. The comparison between
288 the theoretically estimated and literature reported single scattering albedo values showed the percent absolute
289 difference between 1.06% to 5.56%, which validates the proposed Mie theory for estimation of lidar ratio.

290 **4.2 Lidar Ratio for OPAC Aerosol Models Defined in terms of Constituent Components:**

291 The lidar ratios were also estimated when aerosol models were specified in terms of different constituent
292 compositions as used in OPAC. The aerosol models viz. clean continental, average continental, polluted
293 continental, urban, clean maritime, maritime tropical, polluted maritime, desert, arctic and antarctic were used in
294 the present study to estimate the lidar ratio using Mie theory. The number mixing ratios as specified in OPAC
295 software by Hess et al. (1998) were used in the present study to define the size distribution of aerosols. The relative
296 humidity causes an increase in size of a hygroscopic particle such as water soluble, sea salt and sulfate particles.
297 Thus, the backscattering and extinction profiles of these particles are significantly affected.

298   Figure 3 shows the variation in backscatter coefficient of the continental and maritime aerosols at 532 nm and
299   1064 nm. The backscattering coefficient of continental and maritime aerosols were observed to increase when
300   relative humidity was increased from 0% to 99%. The increase in backscattering with relative humidity was
301   considerably higher in polluted continental, urban and polluted maritime aerosols as compared to clean continental
302   and clean maritime aerosols at 532 nm and 1064 nm. Clean maritime and tropical maritime aerosols were observed
303   to have equivalent backscattering coefficients due to their equivalent composition of water soluble and sea salt
304   particles.

305   Figure 4 shows the variation in backscattering coefficients of the desert, arctic and antarctic aerosol models at 532
306   nm and 1064 nm. The Antarctic aerosols showed a sharp and significant increase in their backscattering
307   coefficients at 532 nm and 1064 nm. The increase in backscattering coefficients was observed to be more at 1064
308   nm compared to 532 nm. This causes the decrease in lidar ratio at 1064 nm as compared to that at 532 nm as can
309   be observed from figure 6. Increase in backscattering coefficient with relative humidity at 532 nm and 1064 nm
310   will cause increase or decrease in lidar ratio with respect to relative humidity depending upon the rate at which
311   the extinction and backscattering coefficients are increasing or decreasing.

312   The variation in lidar ratios of continental and maritime aerosol models with reference to relative humidity at 532
313   nm and 1064 nm is as shown in figure 5. The lidar ratio showed an increase in values for polluted continental and
314   polluted maritime aerosols over the clean continental and clean maritime aerosols. This increase was mainly
315   observed due to greater contribution of soot particles in the polluted aerosols. An increase in lidar ratio values was
316   observed at 532 nm and 1064 nm when relative humidity was increased from 80% to 99% in all types of
317   continental and maritime aerosols. The decrease in lidar ratio when relative humidity was increased from 0% to
318   80% was observed due to decrease in lidar ratio of the water soluble particles which are hygroscopic in nature.
319   This decrease was primarily due to significant decrease in the imaginary part of the refractive index of water
320   soluble component due to relative humidity. Continental and Maritime aerosols are dominated by water soluble
321   particles as defined in OPAC and thus an initial decrease and a gradual increase in lidar ratio values was observed
322   at 532 nm and 1064 nm when relative humidity was increased from 0% to 99%.

323   The lidar ratio values of the clean continental model and clean maritime aerosol models at 532 nm and 1064 nm
324   where observed to be centred around 53 sr to 51 sr with varying relative humidity. This is mainly because of the
325   composition of aerosol models as defined in OPAC. In both, clean continental and clean maritime models, water
326   soluble particles were dominant which are smaller in size as compared to the sea salt particles. However, in OPAC
327   the number mixing ratio of sea salt particles which are coarser particles, is very low as compared to finer water
328   soluble particles; which is not the case in CALIPSO clean marine aerosol model. In CALIPSO clean marine
329   model, though coarser particles are more in proportion their contribution to the backscattering and extinction
330   coefficient was observed to be less in magnitude as compared to the fine particles at 532 nm. Thus, the resulting
331   lidar ratio values for CALIPSO aerosol model were centred on 57 sr at 532 nm, which was consistent with the
332   results for OPAC clean maritime aerosol model.

333   The urban aerosols showed a significant increase in the lidar ratio values at 532 nm and 1064 nm compared to
334   other continental aerosols. The dry urban aerosols showed a lidar ratio of 74.88 sr and 61.73 sr at 532 nm and
335   1064 nm respectively; whereas dry clean continental aerosols exhibited the lidar ratio of 53.59 sr and 23.9 sr at
336   532 nm and 1064 nm respectively. This significant increase in lidar ratio values of urban aerosols is primarily due
337   to scattering soot particles. Insoluble particles hardly have any impact on lidar ratio values of urban and continental

338   aerosols due to their very small composition. Similar results were observed when polluted maritime particles were

339   compared to the clean maritime particles.

340   The variation in lidar ratios of desert, arctic and antarctic aerosols with respect to relative humidity is as shown in

341   figure 6. The lidar ratio values at 532 nm were observed to be greater than those at 1064 nm values for desert and

342   antarctic aerosols. The dry desert dust lidar ratio at 532 nm was observed to be 55.32 sr. This result comply with

343   the values for desert dust lidar ratio at 532 nm reported in literature by Muller et al. (2007), Omar et al. (2009),

344   Kim et al. (2018) and Li et al. (2022). The lidar ratio values showed a decrease with relative humidity except the

345   lidar ratio values of antarctic aerosols at 532 nm and 1064 nm. The model of arctic aerosols that is used in the

346   present study is for spring season when the arctic aerosols are mainly the soot particles. Thus, a decrease in lidar

347   ratio values with relative humidity was observed in arctic aerosols as it was in polluted continental and urban

348   aerosols at 1064 nm.

349   The lidar ratio of dry Antarctic aerosols was observed to be 57.73 sr at 532 nm and 20.90 sr at 1064 nm. The

350   summertime model of Antarctic aerosols as defined in OPAC was used in the present study where the Antarctic

351   aerosols are dominated by the sulfate particles. Sulfate particles are hygroscopic in nature with significant large

352   sizes as compared to water soluble particles. The imaginary part of refractive index of sulfate particles in

353   considerably small as compared to water soluble particles at 532 nm and 1064 nm. Thus, a sharp increase in lidar

354   ratio of sulfate particles was observed when relative humidity was increased from 0% to 99% as opposed to

355   continental, maritime and desert aerosol models.

356   **5   Conclusions:**

357   This paper presented a complex theoretical approach for estimating lidar ratio through Mie theory using CALIPSO

358   and OPAC aerosol models. The lidar ratios were estimated at three wavelengths viz. 532 nm, 673 nm and 1064

359   nm. Mie theory estimated lidar ratios at 673 nm were compared with AERONET data-derived lidar ratios at 675

360   nm and Mie theory estimated lidar ratios at 673 nm were observed to lie between the minima and maxima of the

361   AERONET data-derived lidar ratios at 675 nm. Mie theory estimated lidar ratio values for CALIPSO aerosol

362   models were in good agreement with those reported in literature for CALIPSO operational algorithm. Thus,

363   theoretically estimated lidar ratios for CALIPSO aerosol models may be used in future for CALIPSO operational

364   algorithms. CALIPSO aerosol models were specified in terms of number mixing ratio of the fine and coarse

365   particles instead of component particle type and fine particles were observed to have more significant contribution

366   towards extinction and backscattering coefficient despite their low mixing ratio as compared to coarse particles.

367   Thus, Mie theory derived lidar ratio values provide the physical basis for the lidar ratio selection algorithm for

368   derivation of vertical extinction and backscatter particulate profiles using CALIPSO data.

369   The dependence of lidar ratio with relative humidity was analysed using OPAC aerosol models including Arctic

370   and Antarctic aerosols where each aerosol type was identified with the corresponding number mixing ratio of the

371   component particles. The lidar ratio was observed to decrease when relative humidity was increased from 0% to

372   80% and a gradual increase in lidar ratio was observed when relative humidity was increased further to 99%. This

373   phenomenon is the result of dominance of hygroscopic water-soluble particles constituting clean continental, clean

374   marine, tropical continental and desert aerosols. The increase in number mixing ratio of soot particles showed an

375   overall increase in the lidar ratio values of polluted continental, urban and polluted marine aerosols over clean

376 continental and clean marine particles. The soot particles dominate the urban aerosols and arctic aerosols, which

377 are non-hygroscopic fine particles. Thus, a decrease in lidar ratio of urban and arctic aerosols was observed with

378 respect to relative humidity and an increase in the backscattering coefficient of urban and arctic aerosols was

379 observed with relative humidity due to contribution from the hygroscopic water-soluble particles that grows in

380 size in presence of water vapour in the atmosphere. In case of Antarctic aerosols, the lidar ratio was observed to

381 increase with respect to relative humidity due to hygroscopic sulfate particles that backscattered heavily in

382 presence of water vapour.

383 The method presented in this study to estimate the lidar ratio using Mie theory is valid only for spherical, isotropic,

384 non-hygroscopic particles and thus there can be possible errors occurring in the lidar ratio values especially when

385 the aerosols are anisotropic and hygroscopic in nature. Thus, there is future scope for the present study to extend

386 it to theoretical estimation of lidar ratio in case of hygroscopic and anisotropic non-homogeneous particles.

6   Acknowledgement:

7   Competing Interests:
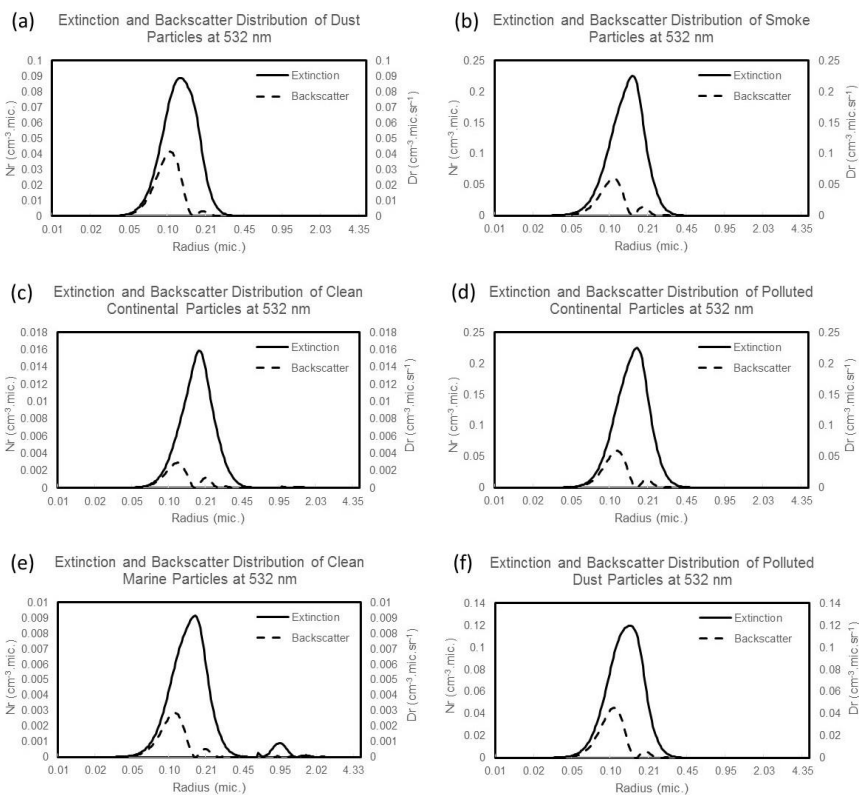
393 This is being declared that none of the authors have any competing interests.

8   References:

395 Ackermann, J.: The Extinction-to-Backscatter Ratio of Tropospheric Aerosol: A Numerical Study, J. Atm. Ocea.

396 Tech., 15, 1043-1050, 1998.

397 Anderson, T. L., Masonis, S. J., Covert, D. S., Charlson, R. J., and Rood, M. J.: In situ measurement of the Aerosol

398 Extinction-to-Backscatter Ratio at a Polluted Continental Site, JGR, 105, 26907-26915, 2000.

399 Ansmann, A., Wagner, F., Müller, D., Althausen, D., Herber, A., von Hoyningen-Huene, W., and Wandinger, U.:

400 European Pollution Outbreaks during ACE 2: Optical Particle Properties Inferred from Multiwavelength Lidar

401 and Star-Sun Photometry, J. Geophys. Res.-Atmos., 107, 8–14, 2002.

402 Bohren, C. F., and Huffman, D. R.: Absorption and Scattering of Light by Small Particles, Wiley and Sons, 530

403 pp., 1983.

404 d'Almeida, G., Koepke, P., and Shettle, E. P.: Atmospheric Aerosols: Global Climatology and Radiative

405 Characteristics, A. Deepak, 561 pp., 1991

406 Dusing, S., Ansmann A., Baars, H., Corbin, J. C., Denjean, C., Gysel-Beer, M., Muller, T., Poulain, L., Siebert,

407 H., Spindler, G., Tuch, T., Wehner, B., and Wiedensohler, B.: Measurement Report: Comparison of Airborne, in-

408 situ Measured, Lidar-based and Modeled Aerosol Optical Properties in the Central European Background –

409 Identifying Sources of Deviations, Atmos. Chem. Phys., 21, 16745-16773, 2021.

410 Hess, M., Koepke, P., and Schult, I.: Optical Properties of Aerosols and Clouds: The Software Package OPAC,
411 Bull. Amer. Meteor. Soc., 79, 831-844, 1998.
412 Kim, M. H., Omar, A. H., Tackett, J. L., Vaughan, M. A., Winker, D. M., Trepte, C. R., Hu, Y., Liu, Z., Poole, L.
413 R., Pitts, M. C., Ka, J., Magill, E.: The CALIPSO version 4 Automated Aerosol Classification and Lidar Ratio
414 Selection Algorithm, Atm. Meas. Tech., 11, 6107-6135, 2018.
415 Li, Z., Painemal, D., Schuster, G., Clayton, M., Ferrare, R. A., Vaughan, M. A., Josset, D., Kar, J., Trepte, C. R.:
416 Assessment of Tropospheric CALIPSO Version 4.2 Aerosol Types over the Ocean using Independent CALIPSO-
417 SODA Lidar Ratios, Atm. Meas. Tech., 15, 2745-2766, 2022.
418 Lopes, F. J. S., Landulfo, E., and Vaughan, M. A.: Evaluating CALIPSO's 532 nm lidar ratio selection algorithm
419 using AERONET sun photometers in Brazil, Atmos. Meas. Tech., 6, 3281-3299, 2013.
420 Muller, D., Ansmann, A., Mattis, I., Tesche, M., Wandinger, U., Althausen, D., and Pisani, G. : Aerosol-type-
421 dependent Lidar Ratios Observed with Raman Lidar, JGR, 112, D16202, 2007.
422 Omar, A. H., Won, J. G., Winker, D. M., Yoon, S. C., Dubovik, O., and McCormick, M. P.: Development of
423 Global Aerosol Models using Cluster Analysis of Aerosol Robotic Network (AERONET) Measurements, JGR,
424 110, 1-14, 2005.
425 Omar, A. H., Winker, D. M., Kittaka, C., Vaughan, M. A., Liu, Z., Hu, Y., Trepte, C. R., Rogers, R. R., Ferrare,
426 R. A., Lee, K. P., Kuehn, R. E., and Hostetler, C. A.: The CALIPSO Automated Aerosol Classification and Lidar
427 Ratio Selection Algorithm, J. Atm. Ocea. Tech., 26, 1994-2014, 2009.
428 Salemink, H., Schotanus, P., and Bergwerff, J. B.: Quantitative Lidar at 532 nm for Vertical Extinction Profiles
429 in the Lidar Solution, Appl. Phys., 34B, 187–189, 1984.
430 Takamura, T., Sasano Y., and Hayasaka T.: Tropospheric Aerosol Optical Properties Derived from Lidar, Sun
431 Photometer, and Optical Particle Counter Measurements, Appl. Opt., 33, 7132–7140, 1994.
432 Vermote, E. F., Tanre, D., Deuze, J. L., Herman, M., Morcrette, J. J., Kotchenova, S. Y.: Second Simulation of a
433 Satellite Signal in the Solar Spectrum – Vector (6SV) User Guide Version 3 – Part II, available at
434 (http://6s.ltdri.org/), 2006.
435 Young, S. A. and Vaughan, M. A.: The Retrieval of Profiles of Particulate Extinction from Cloud-Aerosol Lidar
436 Infrared Pathfinder Satellite Observations (CALIPSO) data: Algorithm Description, J. Atm. Ocea. Tech., 26,
437 1105-1119, 2009.
438 Zhao, G., Zhao, C., Kuang, Y., Tao, J., Tan, W., Bian, W., Li, J. and Li, C.: Impact of Aerosol Hygroscopic
439 Growth on Retrieving Aerosol Extinction Coefficient Profiles from Elastic-Backscatter Lidar Signals, Atmos.
440 Chem. Phys., 17, 12133-12143, 2017.
441
442

443

444

445
446
447

Figure 1: Extinction and Backscatter Distribution at 532 nm of CALIPSO Aerosol Models viz. (a) Dust (b) Smoke (c) Clean Continental (d) Polluted Continental (e) Clean Marine and (f) Polluted Dust

448

449

450

451

452

453

454

455
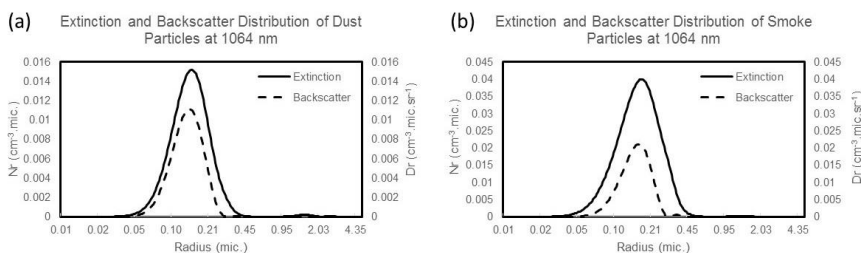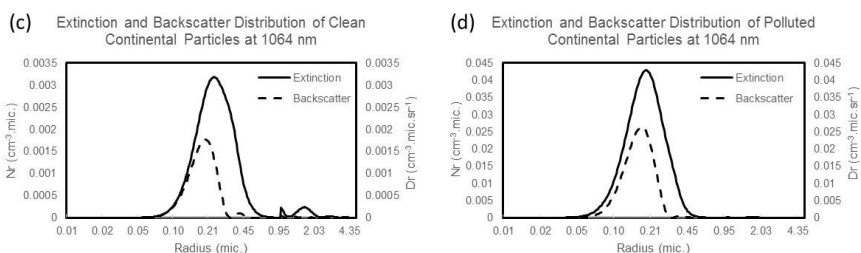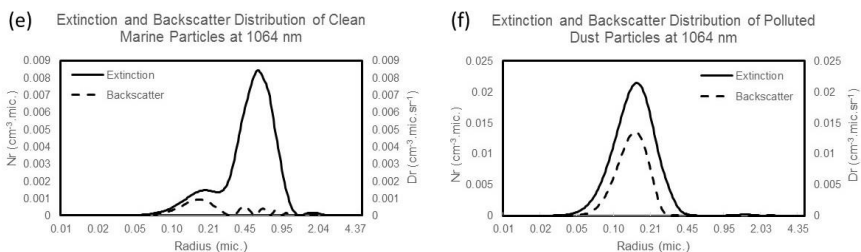
Figure 2: Extinction and Backscatter Distribution at 1064 nm of CALIPSO Aerosol Models viz. (a) Dust (b) Smoke (c) Clean Continental (d) Polluted Continental (e) Clean Marine and (f) Polluted Dust
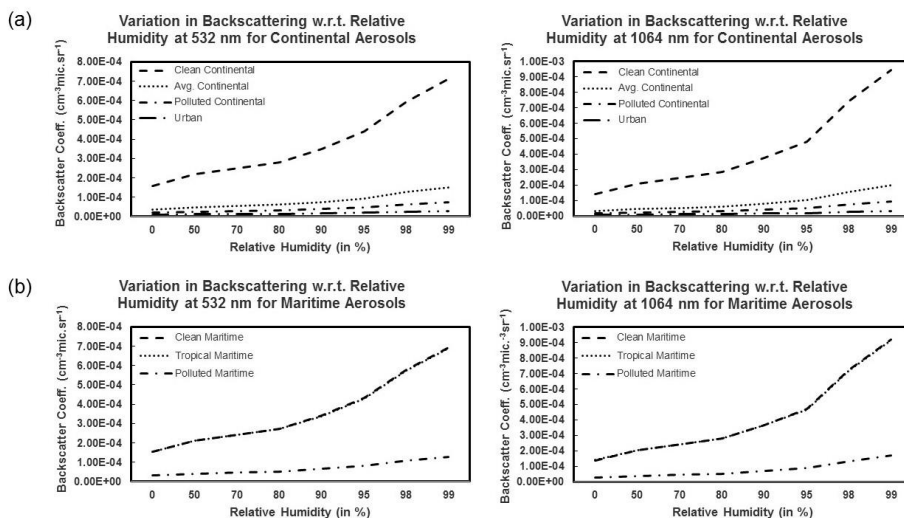
Figure 3: Variation in Backscattering Coefficient w.r.t. Relative Humidity for (a) Continental Aerosols and (b) Maritime Aerosols at 532 nm and 1064 nm.

Atmospheric
Measurement
Techniques

Discussions

464

465

Figure 4: Variation in Backscattering Coefficient w.r.t. Relative Humidity for (c) Desert Aerosols and (d) Arctic Aerosols and (e) Antarctic Aerosols at 532 nm and 1064 nm.

468

469
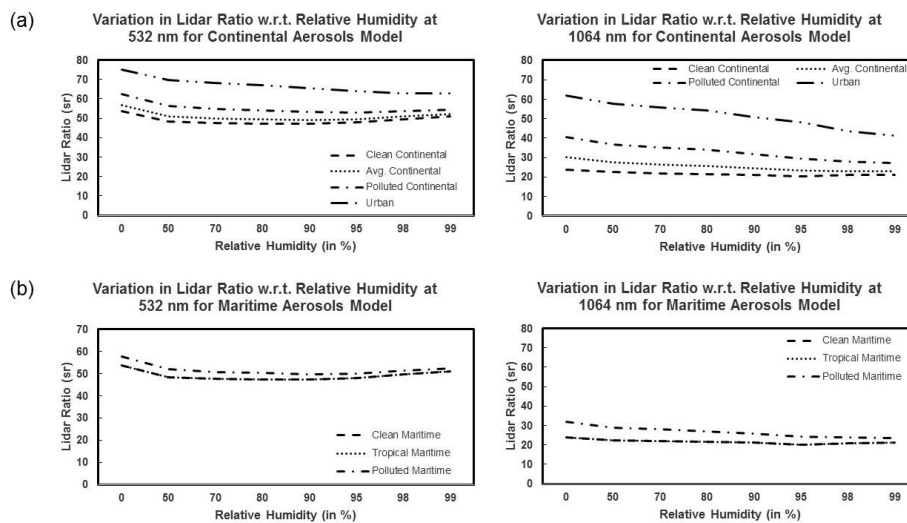
Figure 5: Variation in Lidar Ratio w.r.t. Relative Humidity for (a) Continental Aerosols and (b) Maritime Aerosols at 532 nm and 1064 nm.
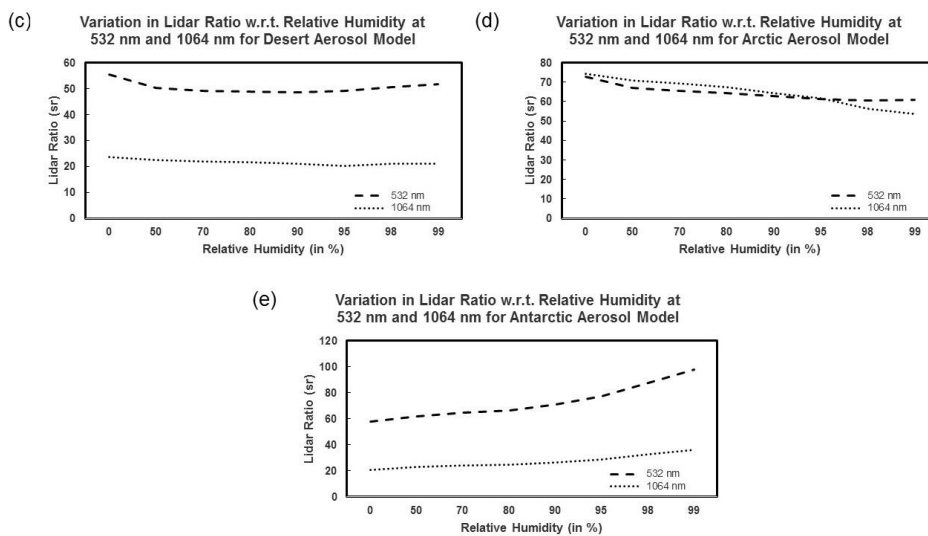
Figure 6: Variation in Lidar Ratio w.r.t. Relative Humidity for (c) Desert Aerosols and (d) Arctic Aerosols and (e) Antarctic Aerosols at 532 nm and 1064 nm.

Atmospheric
Measurement
Techniques

Discussions

493   **Table 1**: Physical and Optical Properties of CALIPSO Aerosol Models (Omar et al. 2009)

Aerosol	$m_{r,532}$	$m_{i,532}$	$m_{r,1064}$	$m_{i,1064}$	$r_{m,fine}$	σ_{fine}	$r_{m,coarse}$	σ_{coarse}	μ_{fine}
Dust	1.414	0.0036	1.495	0.0043	0.1165	1.4813	2.8329	1.9078	0.223
Smoke	1.517	0.0234	1.541	0.0298	0.1436	1.5624	3.7260	2.1426	0.329
Clean Continental	1.380	0.0001	1.380	0.0001	0.20556	1.6100	2.6334	1.8987	0.050
Polluted Continental	1.404	0.0063	1.439	0.0073	0.1577	1.5257	3.5470	2.0650	0.531
Clean Marine	1.400	0.0050	1.400	0.0050	0.1500	1.6000	1.2160	1.6000	0.025
Polluted Dust	1.452	0.0109	1.512	0.0137	0.1265	1.5112	3.1617	1.9942	0.241

494

495   **Table 2**: Physical and Optical Properties of AERONET Aerosol Models at 673 nm classified using Cluster
496   Analysis (Omar et al. 2005)

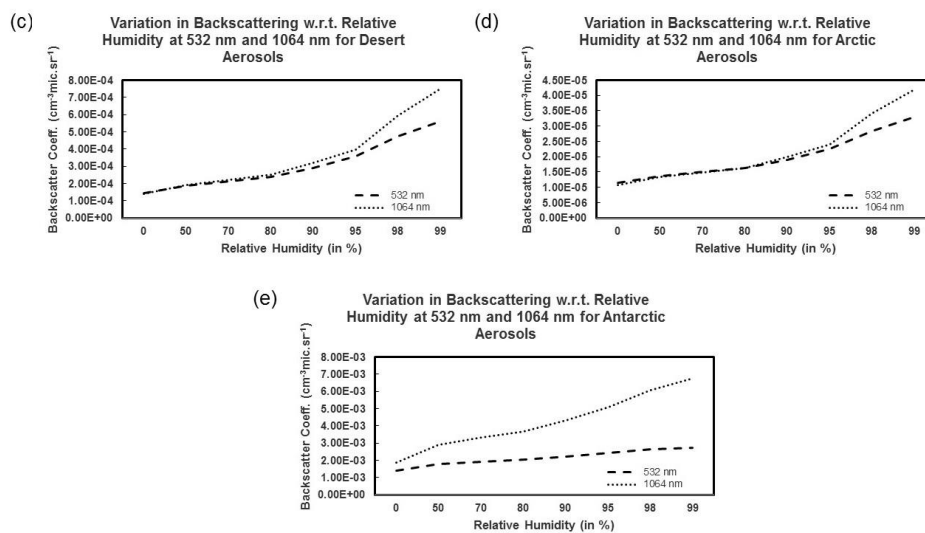| Aerosol	$m_{r,673}$	$m_{i,673}$	$r_{m,fine}$	σ_{fine}	$r_{m,coarse}$	σ_{coarse}	μ_{fine}
Category 1	1.4520	0.0036	0.117	1.482	2.834	1.908	0.22
Category 2	1.5202	0.0245	0.144	1.562	3.733	2.144	0.33
Category 3	1.4494	0.0092	0.133	1.502	3.590	2.104	0.38
Category 4	1.4098	0.0063	0.158	1.526	3.547	2.065	0.53
Category 5	1.3943	0.0044	0.165	1.611	3.268	1.995	0.26
Category 6	1.4104	0.0337	0.140	1.540	3.556	2.134	0.49

497

498   **Table 3**: Size Distribution of Aerosol Components for Models used in OPAC for Different Relative Humidities
499   (d'Almeida et al. 1991 and Ackermann 1998)

Component	r_m (0%)	r_m (50%)	r_m (70%)	r_m (80%)	r_m (90%)	r_m (95%)	r_m (98%)	r_m (99%)	σ
Water Soluble	0.0212	0.0262	0.0285	0.0306	0.0348	0.0399	0.0476	0.0534	2.239
Insoluble	0.4710	0.4710	0.4710	0.4710	0.4710	0.4710	0.4710	0.4710	2.512
Soot	0.0118	0.0118	0.0118	0.0118	0.0118	0.0118	0.0118	0.0118	2.000
Mineral (nuc.)	0.0700	0.0700	0.0700	0.0700	0.0700	0.0700	0.0700	0.0700	1.950
Mineral (acc.)	0.3900	0.3900	0.3900	0.3900	0.3900	0.3900	0.3900	0.3900	2.000
Mineral (coa.)	1.9000	1.9000	1.9000	1.9000	1.9000	1.9000	1.9000	1.9000	2.150
Mineral (trans.)	0.5000	0.5000	0.5000	0.5000	0.5000	0.5000	0.5000	0.5000	2.200
Sea Salt (acc.)	0.2090	0.3360	0.3780	0.4160	0.4970	0.6050	0.8010	0.9950	2.030
Sea Salt (coa.)	1.7500	2.8200	3.1700	3.4900	4.1800	5.1100	6.8400	8.5900	2.030
Sulfate	0.0695	0.0983	0.1090	0.1180	0.1350	0.1580	0.1950	0.2310	2.030

500

501

Atmospheric
Measurement
Techniques
Open Access
Discussions
EGU

502 **Table 4**: Refractive Indices of the Aerosol Components for the OPAC Aerosol Models used in this study
503 (d'Almeida et al. 1991 and Ackermann 1998)

Component	$m_{r,532}$	$m_{i,532}$	$m_{r,1064}$	$m_{i,1064}$
Water Soluble	1.530	5.64×10^{-3}	1.520	1.64×10^{-2}
Insoluble	1.530	8.0×10^{-3}	1.510	8.00×10^{-3}
Soot	1.750	4.46×10^{-1}	1.760	4.43×10^{-1}
Mineral	1.530	6.33×10^{-3}	1.530	4.30×10^{-3}
Sea Salt	1.500	1.12×10^{-8}	1.470	1.95×10^{-4}
Sulfate	1.430	1.00×10^{-8}	1.423	1.50×10^{-6}
Water	1.333	1.61×10^{-9}	1.326	1.39×10^{-5}

504

505 **Table 5**: Composition of Aerosol Models used in OPAC (Hess et al. 1998)

Aerosol Types	Components	Number Mixing Ratio μ_i
Clean Continental	Water soluble	1.000
	Insoluble	0.577×10^{-4}
Average Continental	Water Soluble	0.458
	Insoluble	0.261×10^{-4}
	Soot	0.542
Polluted Continental	Water Soluble	0.314
	Insoluble	0.120×10^{-4}
	Soot	0.686
Urban	Water Soluble	0.177
	Insoluble	0.949×10^{-5}
	Soot	0.823
Clean Maritime	Water Soluble	0.987
	Sea Salt (acc.)	0.132×10^{-1}
	Sea Salt (coa.)	0.211×10^{-5}
Tropical Maritime	Water Soluble	0.983
	Sea Salt (acc.)	0.167×10^{-1}
	Sea Salt (coa.)	0.217×10^{-5}
Polluted Maritime	Water Soluble	0.422
	Sea Salt (acc.)	0.222×10^{-2}
	Sea Salt (coa.)	0.356×10^{-6}
	Soot	0.576
Desert	Water Soluble	0.870
	Mineral (nuc.)	0.117
	Mineral (acc.)	0.133×10^{-1}
	Mineral (coa.)	0.617×10^{-4}
Arctic	Water Soluble	0.197
	Insoluble	0.152×10^{-5}
	Sea Salt (acc.)	0.288×10^{-3}
	Soot	0.803
Antarctic	Sulfate	0.998
	Sea Salt (acc.)	0.109×10^{-2}
	Mineral (trans.)	0.123×10^{-3}

506

507

Atmospheric
Measurement
Techniques
Open Access
Discussions

508

Table 6: Lidar Ratio (in sr) estimated using Mie theory for Omar et al. (2005) Aerosol Models

Aerosol Model	Desert Dust (Category-1)	Biomass Burning (Category -2)	Rural (Background) (Category-3)	Industrial Pollution (Category-4)	Polluted Marine (Category-5)	Dirty Pollution (Category- 6)
673 nm	28.68	46.92	36.27	44.20	45.18	48.87

510

Table 7: Lidar Ratio (in sr) Comparison between Theoretical values estimated using Mie Theory and In-situ values using Category-1 AERONET Data

Site/Year	2017	2018	2019	2020	2021	Mie Theory Estimate
Kanpur	53.67	47.32	50.31	54.12	50.46	28.68
Min.	36.06	21.31	30.76	32.03	29.41	
Max.	92.52	78.92	86.23	83.53	79.75	
	1998	**1999**	**2004**	**2005**	**2006**	
Bahrain	47.82	37.00	40.79	37.66	34.88	28.68
Min.	37.40	28.32	31.43	27.78	27.68	
Max.	69.67	81.69	53.60	64.40	45.83	
	2017	**2018**	**2019**	**2020**	**2021**	
Banizoumbou	49.96	52.04	50.98	49.88	51.12	28.68
Min.	27.80	29.08	37.20	32.10	41.83	
Max.	65.81	67.73	70.83	70.75	72.14	

513

Table 8: Lidar Ratio (in sr) Comparison between Theoretical values estimated using Mie Theory and In-situ values using Category-2 AERONET Data

Site/Year	2001	2002	2003	2004	2005	Mie Theory Estimate
Abracos Hill	52.95	53.89	51.87	50.52	55.30	46.92
Min.	44.99	41.63	32.30	44.24	39.87	
Max.	60.44	66.43	63.01	57.72	65.54	
	2016**	**2017**	**2018**	**2019**	**2020***	
Skukuza	38.47	49.37	43.01	44.04	63.24	46.92
Min.	19.14	32.50	34.98	28.56	63.24	
Max.	49.70	101.24	52.74	68.14	63.24	
	2014	**2015**	**2016**	**2017**	**2018**	
IMS Metu Erdemli	54.47	42.50	51.24	58.80	49.26	46.92
Min.	22.54	27.64	31.90	35.90	27.83	
Max.	69.72	61.70	73.60	75.06	67.43	

*Only single data value is available
**The data has an outlier. Without outlier the value of LR is 43.30 sr.

518

519

520

521

Atmospheric
Measurement
Techniques
Open Access
Discussions
EGU

Table 9: Lidar Ratio (in sr) Comparison between Theoretical values estimated using Mie Theory and In-situ values using Category-3 AERONET Data

Site/Year	2002	2003	2005	2006	2009*	Mie Theory Estimate
Konza EDC	52.25	43.95	54.47	39.38	47.83	36.27
Min.	39.64	32.40	37.32	38.32	35.30	
Max.	64.46	73.75	85.26	40.45	58.52	
	2012	2017	2018	2020	2021**	
Sevilleta	44.47	48.17	42.10	58.52	53.53	36.27
Min.	34.65	37.09	31.75	33.45	27.39	
Max.	56.64	57.99	56.59	78.83	72.29	
	2015	2017	2018	2020	2021	
Rimrock	46.45	49.98	47.41	47.43	47.65	36.27
Min.	37.53	35.03	29.97	39.36	33.47	
Max.	52.55	60.36	57.35	58.93	63.86	

*Only two data values are available

**The data has an outlier. Without outlier the value of LR is 50.40 sr.

Table 10: Lidar Ratio (in sr) Comparison between Theoretical values estimated using Mie Theory and In-situ values using Category-4 AERONET Data

Site/Year	2009	2012	2013	2014	2015	Mie Theory Estimate
Mexico City	54.44	56.86	56.99	64.40	63.40	44.20
Min.	23.16	37.61	39.66	47.48	36.68	
Max.	87.92	77.17	91.83	81.93	99.16	
	2003	2004	2005	2006	2007	
Moscow MSU MO	55.28	57.45	53.84	43.03	49.61	44.20
Min.	46.25	43.76	37.77	30.15	33.79	
Max.	68.83	71.03	77.44	55.44	68.28	
	2015	2016	2017	2018	2019	
GSFC	59.15	55.56	53.15	58.07	52.68	44.20
Min.	39.82	47.01	50.18	40.18	40.04	
Max.	67.93	60.78	55.15	68.84	61.79	

Table 11: Lidar Ratio (in sr) Comparison between Theoretical values estimated using Mie Theory and In-situ values using Category-5 AERONET Data

Site/Year	2002	2003	2011*	2012	2013	Mie Theory Estimate
Arica	62.45	69.22	67.68	73.63	62.94	45.18
Min.	44.66	52.14	67.68	69.62	41.86	
Max.	90.27	86.74	67.68	76.62	77.02	
	2004	2005	2007	2008	2009	
La Parguera	47.91	51.00	45.00	47.64	46.38	45.18
Min.	45.70	48.91	37.10	45.12	39.01	
Max.	50.72	56.92	51.73	50.99	52.49	
	2013	2014	2015	2016	2017	
Ascension Island	54.55	55.31	59.29	52.54	70.73	45.18
Min.	43.57	50.08	36.15	41.35	48.15	
Max.	67.64	62.07	74.13	67.57	92.67	

*Only single data value is available

Atmospheric
Measurement
Techniques
Discussions

531 **Table 12**: Lidar Ratio (in sr) Comparison between Theoretical values estimated using Mie Theory and In-situ
532 values using Category-6 AERONET Data

Site/Year	2017	2018	2019	2020*	2021	Mie Theory Estimate
Dalanzadgad	52.80	41.68	47.58	37.85	47.43	48.87
Min.	39.46	32.05	41.55	37.85	38.27	
Max.	66.15	51.32	50.77	37.85	56.60	
	2016**	**2017**	**2018**	**2019**	**2020***	
Skukuza	38.47	49.37	43.01	44.04	63.24	48.87
Min.	19.14	32.50	34.98	28.56	63.24	
Max.	49.70	101.24	52.74	68.14	63.24	
	2014	**2015**	**2016**	**2017**	**2018**	
IMS Metu Erdemli	54.47	42.50	51.24	58.80	49.26	48.87
Min.	22.54	27.64	31.90	35.90	27.83	
Max.	69.72	61.70	73.60	75.06	67.43	

533 *Only single data value is available
534 **The data has an outlier. Without outlier the value of LR is 43.30 sr.

535

536 **Table 13**: Lidar Ratio (in sr) for Aerosol Models in CALIPSO Operational Algorithm

Wavelength/ Aerosol Model	Dust	Smoke (Biomass Burning)	Clean Continental	Polluted Continental	Clean Marine	Polluted Dust
Omar et al. (2009) CALIPSO V1 (based on in-situ measurements)						
532 nm	40	70	35	70	20	65
1064 nm	55	40	30	40	45	30
Lopes et al. (2013) CALIPSO LR Selection Algo. Evaluation (Mean ± S.D.)						
532 nm	40 ± 20	70 ± 28	35 ± 16	70 ± 25	20 ± 6	55 ± 22
Kim et al. (2018) CALIPSO V3 Operational Algo. (based on in-situ measurements)						
532 nm	40 ± 20	70 ± 25	35 ± 16	70 ± 25	20 ± 6	55 ± 22
1064 nm	55 ± 17	30 ± 14	30 ± 17	30 ± 14	45 ± 23	48 ± 24
Kim et al. (2018) CALIPSO V4 Operational Algo. (based on in-situ measurements)						
532 nm	44 ± 9	70 ± 25	53 ± 24	70 ± 25	23 ± 5	55 ± 22
1064 nm	44 ± 13	30 ± 14	30 ± 17	30 ± 14	23 ± 5	48 ± 24
Li et al. (2022) CALIPSO LR Selection Algo. Evaluation using SODA (Mean ± S.D.)						
532 nm (D)	42 ± 19	45 ± 17	-	45 ± 17	33 ± 15	52 ± 19
532 nm (N)	37 ± 13	57 ± 18	-	57 ± 18	33 ± 16	51 ± 18
In-house Derived in this study using Mie Theory						
532 nm	**38.72**	**63.37**	**85.98**	**64.73**	**57.31**	**48.22**
1064 nm	**20.11**	**33.68**	**31.98**	**26.44**	**71.11**	**25.56**

537

538

539